Appl Biochem Biotechnol
DOI 10.1007/s12010-009-8606-z

Rheology of Dilute Acid Hydrolyzed Corn Stover at High Solids Concentration

M. R. Ehrhardt · T. O. Monz · T. W. Root · R. K. Connelly · C. T. Scott · D. J. Klingenberg

Received: 8 December 2008 / Accepted: 9 March 2009

Abstract The rheological properties of acid hydrolyzed corn stover at high solids concentration (20–35 wt.%) were investigated using torque rheometry. These materials are yield stress fluids whose rheological properties can be well represented by the Bingham model. Yield stresses increase with increasing solids concentration and decrease with increasing hydrolysis reaction temperature, acid concentration, and rheometer temperature. Plastic viscosities increase with increasing solids concentration and tend to decrease with increasing reaction temperature and acid concentration. The solids concentration dependence of the yield stress is consistent with that reported for other fibrous systems. The changes in yield stress with reaction conditions are consistent with observed changes in particle size. This study illustrates that torque rheometry can be used effectively to measure rheological properties of concentrated biomass.

Keywords Biomass · Corn stover · Rheology · Yield stress · Viscosity · Acid hydrolysis

Introduction

Biomass refining typically involves numerous steps. In a process developed by the National Renewable Energy Laboratory (NREL) for the conversion of corn stover to ethanol [1, 2], the biomass is first "pretreated" using dilute acid hydrolysis at elevated temperature in order

M. R. Ehrhardt · T. O. Monz · T. W. Root · D. J. Klingenberg (✉)
Department of Chemical and Biological Engineering, University of Wisconsin, Madison, WI 53706, USA
e-mail: klingen@engr.wisc.edu

M. R. Ehrhardt · T. O. Monz · T. W. Root · D. J. Klingenberg
Rheology Research Center, University of Wisconsin, Madison, WI 53706, USA

R. K. Connelly
Department of Biological Systems Engineering, University of Wisconsin, Madison, WI 53706, USA

R. K. Connelly
Department of Food Science, University of Wisconsin, Madison, WI 53706, USA

C. T. Scott
US Forest Service Forest Products Laboratory, Madison, WI 53706, USA

Published online: 31 March 2009

to make the cellulose more accessible. The cellulose is then enzymatically hydrolyzed to produce glucose. The glucose is subsequently fermented to produce an ethanol solution; the ethanol is then purified in several separation steps. Commercialization of such processes requires reducing the processing costs [3–5].

The cost of processing biomass can be reduced by increasing the concentration of insoluble solids in the various operations [6–8]. However, increasing the solid concentration increases the apparent viscosity of the biomass, which makes mixing and transporting the biomass more challenging [9–11]. It is, thus, apparent that optimization of biomass processes will benefit from understanding the factors that affect the rheology of the biomass.

Pimenova and Hanley [12, 13] measured the apparent rheological properties of pretreated corn stover suspensions (average fiber length 120 μm) using a Brookfield viscometer with a helical impeller. The shear stress–shear rate data exhibited plastic-type rheological behavior with an apparent yield stress. The yield stress increased with solids concentration, but no information about the dependence of rheological properties on pretreatment conditions was reported. The authors also noted that the helical impeller technique is not appropriate for concentrated slurries (solids mass fraction >32%).

Rosgaard et al. [9] investigated the effect of solid content and enzymatic hydrolysis on the apparent viscosity of barley straw biomass slurries, with solid mass fractions varying from 5 to 15 wt.%. The apparent viscosity increased with solid mass fraction and decreased with time during enzymatic hydrolysis.

More recently, Viamajala et al. [14] examined the rheology of acid hydrolyzed corn stover at high solids concentrations (10–40 wt.%) using a Brookfield viscometer with parallel disks. The corn stover was finely milled using a Wiley mill. The authors also found that the corn stover slurries behaved like yield stress fluids, with yield stresses that decrease with increasing hydrolysis temperature and decreasing particle size. The authors also found that the yield stress increased with solids concentration up to a point and then became independent of concentration at high concentrations. The reason for the plateau at high concentrations is not clear.

In this report, we describe the effects of solids concentration (20–35 wt.%) and prehydrolysis reaction conditions on the rheological properties of corn stover slurries. At such high concentrations, these materials are very viscous. Measuring rheological properties and extracting parameters such as a yield stress can be challenging [15]. We use torque rheometry to characterize the rheological properties of the concentrated corn stover slurries. We have previously found torque rheometry to be an effective method for characterizing the rheological behavior of highly viscous wood fiber suspensions for extrusion [16–18]. For the corn stover studied here, the steady-state rheological properties are well described by the Bingham model, with a yield stress that increases with solids concentration, consistent with that reported by Pimenova and Hanley [12, 13] and Viamajala et al. [14]. However, yield stress values reported here are significantly larger than those reported by Pimenova and Hanley and Viamajala et al. This difference is attributed in part to larger particle sizes employed in the present study. Yield stresses decrease with increasing pretreatment reaction temperature and acid concentration.

Materials and Methods

The methods and materials are described briefly here. More details are available elsewhere [19].

Baled, dried corn stover was obtained from the University of Wisconsin Arlington Research Station in August 2007. The particle size was reduced by processing the corn stover in a hammer mill (27 in. diameter, 7/8 in. screen, 15 hp, 2,500 rpm). The hammer-

milled corn stover was screened and washed to remove dirt while maximizing fines recovery. The particle size distribution was characterized by screening 1 kg of corn stover over a stack of screens. The amount of material retained on each screen is plotted as a function of screen opening size in Fig. 1.

Dilute-acid hydrolysis reactions were performed in 2- or 20-l stainless steel, jacket-heated, glass-lined Parr reactors. The internal temperature was measured with a thermocouple near the reactor wall and a thermocouple in the center of the biomass sample. The temperature was controlled using a Parr 4843 controller connected to the outer thermocouple.

The dilute-acid hydrolysis procedure is based on NREL Laboratory Analytical Procedure 007 (LAP-007) [20]. All hydrolysis reactions were performed at 10 wt.% dry solids. The appropriate amount of biomass was first added to the reactor. Dilute sulfuric acid was then poured slowly over the biomass and stirred, ensuring that all of the material was wetted.

Because of the finite rate of heat transfer from the jacket to the biomass, the heating rate must be small to prevent a large temperature difference between the biomass near the wall and near the center. The heating rate was adjusted to maintain a temperature difference between the wall and the center of less than 10 °C. When the mean internal temperature of the reactor reached the target temperature, the reaction was considered to start. For the 2-l reactor, quenching in a cold water bath was started once the target reaction time was reached. For the 20-l reactor, quenching began 10 min before the target reaction time was reached because of the slower cooling.

Following dilute-acid hydrolysis, the biomass was washed and neutralized prior to rheological and particle size analysis. Vacuum filtration was used to wash the biomass, with each 200–300 g sample (wet basis) washed with 1,000 g water. The liquid fraction was weighed and stored in a covered 5-gal pail at approximately 10 °C. The solid fraction was weighed and the solids concentration determined.

The solids fraction of each dilute-acid hydrolysis reaction was neutralized with a $NaHCO_3$ solution following the washing step. The solids fraction was added to a 10-g/L $NaHCO_3$ solution with 0.2 g $NaHCO_3$ used for every 1.0 g dry biomass. This slurry was allowed to sit for several minutes then vacuum filtered with each 200–300 g sample (wet basis) washed with 1 l water. This procedure resulted in a biomass sample with pH greater than 6, which was confirmed using pH paper. The recovered solids were then sealed and stored at 10 °C.

The temperature during the dilute-acid hydrolysis varies continuously with time. The temperature profile can be characterized by an effective temperature, following the so-

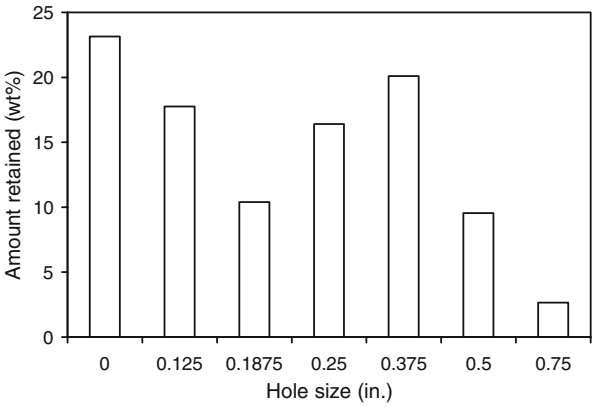

Fig. 1 Amount of corn stover (hammer milled, prior to hydrolysis) retained on screens in a screen stack as a function of screen opening size

called H factor analysis devised by Vroom [21, 22]. In this analysis, a temperature-dependent relative reaction rate constant is expressed

$$k = \exp\left[\frac{-E_a}{R}\left(\frac{1}{T} - \frac{1}{373}\right)\right], \tag{1}$$

where k is the reaction rate constant relative to the value at 100 °C (373 K), E_a is the activation energy, R is the gas constant, and T is the temperature in Kelvin. For this study, activation energy of 120 kJ/mol was chosen based on previous work [23–27].

The H factor is defined

$$H = \int_0^{t_{rxn}} k(T)dt \tag{2}$$

where t_{rxn} is the target reaction time. The H factor, which is evaluated numerically from the experimentally measured mean internal temperature profile, represents the overall extent of reaction relative to the extent of a dilute-acid hydrolysis reaction at 100 °C at an equal reagent concentration. The effective reaction temperature T_{eff} is defined as the constant temperature that would provide an equivalent extent of reaction over the target reaction time,

$$T_{eff} = \left[\frac{1}{373} - \frac{R}{E_a}\ln\left(\frac{H}{t_{rxn}}\right)\right]^{-1}. \tag{3}$$

The solids content of biomass samples were determined by dispersion in water, vacuum filtration, and drying. A 15–20-g wet basis biomass sample was mixed with approximately 500 mL water with a vertical air-driven impeller. The solids were removed from this slurry by vacuum filtration using dried and weighed filter paper. Collected solids and the filter paper were dried in a press drier at 315 °C until the sample mass no longer changed with time. Solids content was determined by dividing the dry sample mass less the filter paper mass by the initial wet biomass weight.

The solids content of biomass samples was increased by pressing the material between paper blotters. For increases of solids content up to 25 wt.%, the material was pressed by hand between two blotters and weighed. For increases beyond 25 wt.%, the material was pressed between four blotters with a hydraulic press. In all cases, the mass lost to the blotters is assumed to be water.

Rheological analysis was performed using a torque rheometer (Brabender Plasticorder) illustrated in Fig. 2. The rheometer consists of a brass mixing chamber with two equally sized cylindrical volumes where chrome-plated steel impellers counter-rotate to impose shear on the biomass. Between the cylindrical shear zones, there is a mixing zone where material can pass from one cylinder to the other. One impeller rotates at the input shaft speed (impeller 1) while the other turns at two thirds of the input speed (impeller 2). The temperature of the mixing chamber is controlled by water flowing through a channel around the chamber. Total shaft torque is measured with a magnetoelastic sleeve torque transducer connected to the motor shaft and recorded at 5 Hz. Both water temperature and chamber internal temperature are measured using thermocouples, with the internal chamber thermocouple enclosed in a thermowell inserted into the top of the chamber.

To perform rheological measurements, the mixing chamber is completely filled with the test material. During sample addition, the shaft is turned by hand to expose air bubbles, which are then removed by adding more material. Once the chamber is full, the water temperature is adjusted to attain the desired test temperature. Mixing and data acquisition for torque and temperature begin when the internal temperature is within 5 °C of the target temperature, as mixing causes the internal temperature to equilibrate rapidly.

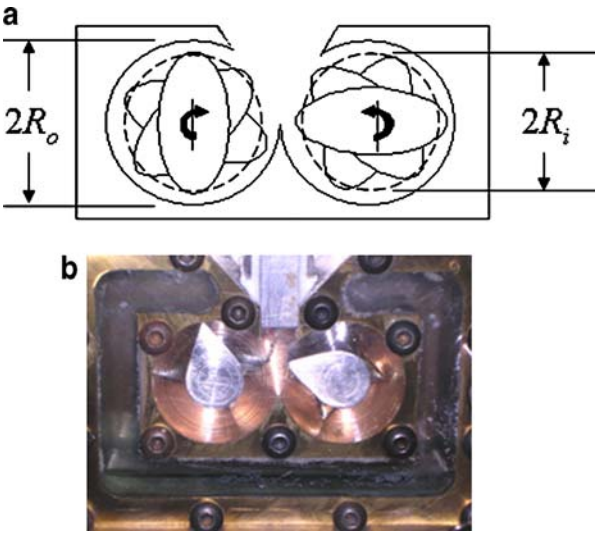

Fig. 2 **a** Schematic diagram of the torque rheometer. **b** Photograph of the torque rheometer chamber

For the experiments reported here, the torque rheometer measurements were performed as follows. The input shaft speed was first maintained at 220 rpm for 600 s. This step is employed to help reach a steady measured torque. The input shaft speed was then cycled through a series of steps, with increasing and decreasing shaft speeds: the speed was held for 100 s at each of 55, 110, 220, 110, and 55 rpm to obtain torque data at each of these rotation rates. This sequence of steps was repeated two to four times (other input speeds, such as 28 and 165 rpm, were occasionally added to the sequence of steps). Unless specifically stated otherwise, measurements were performed at 55 °C.

The effect of rheometer temperature on rheological properties was investigated in some runs. Immediately after the step sequence described above, the temperature was changed to different steady values and the torque was measured for a sequence of decreasing shaft speeds.

Torque–rotation rate data were converted to conventional rheological quantities using a calibration procedure developed by Goodrich and Porter [28]. The torque rheometer is represented by two sets of concentric cylinders. The outer cylinder radius R_o is equated with the actual cylindrical bowl radius. The effective inner radius R_i is determined by equating the measured torque for a Newtonian fluid with known viscosity with that calculated from the solution of the Navier–Stokes equation. Bousmina et al. [29] showed that such a calibration with a Newtonian fluid gives equivalent results to that obtained using a more sophisticated analysis with power-law fluids.

Once the effective inner radius is obtained, the torque (Γ) and rotation rate (Ω) data can be transformed into apparent shear stress (τ) and apparent shear rate ($\dot{\gamma}$) data for the fast impeller (impeller 1) for a torque rheometer with a 3:2 drive-to-driven gear ratio via

$$\tau = \frac{9}{13}\frac{\Gamma}{2\pi R_a^2 h}, \tag{4}$$

$$\dot{\gamma} = \frac{2R_i R_o \Omega}{\left(\frac{1}{\kappa} - \kappa\right)}\frac{1}{R_a^2}, \tag{5}$$

where $R_a \equiv (R_i + R_o)/2$ is the midpoint radius, h is the impeller depth, and $\kappa \equiv R_i/R_o$. This approach is consistent with that employed in commercial rheometers [30]. To extract rheological parameters such as a yield stress, one can simply fit the torque–rotation rate data to that predicted for a particular constitutive model. We follow this approach, employing the Bingham model, where the local stress τ_{loc} related to the local shear rate $\dot{\gamma}_{loc}$ by

$$\tau_{loc} = \tau_0 + \eta_{pl}\dot{\gamma}_{loc}, \tag{6}$$

where τ_0 is the yield stress and η_{pl} is the plastic viscosity. The predicted torque is $\Gamma = \Gamma_1 + (2/3)\Gamma_2$, where the torque–rotation rate relationship for concentric cylinder geometry k is (k=1,2)

$$\Gamma_k = 4\pi R_i^2 h \left[\frac{\Omega_k + \frac{\tau_0}{\eta_{pl}} \ln\left(\frac{r_0}{R_i}\right)}{1 - \frac{R_i^2}{r_0^2}} \right], \tag{7}$$

and where r_0 is the location of the radius at which the velocity goes to zero, determined by solution of

$$\left(\frac{r_0}{R_i}\right)^2 - 1 = \frac{2\eta_{pl}\Omega_k}{\tau_0} + \ln\left[\left(\frac{r_0}{R_i}\right)^2\right]. \tag{8}$$

For $r_0 > R_o$, the torque is given by Eq. 7 with r_0 replaced by R_o. Thus, by fitting the above model for the predicted torque to experimental torque–rotation rate data, the yield stress and plastic viscosity can be extracted. For this fitting procedure, we employ a Gauss–Newton method to minimize the error between the measured and predicted torques [12]. We note that Eqs. 7 and 8 reveal that for the torque rheometer geometry, the torque is not a linear function of the rotation rate for the Bingham model; therefore, the apparent shear stress (Eq. 4) is not a linear function of the apparent shear rate (Eq. 5).

Results and Discussion

Typical torque rheometry results are illustrated in Fig. 3 for hammer milled corn stover hydrolyzed at T_{eff}=182 °C for 30 min with 0.5 wt.% H_2SO_4. Here, the torque (averaged over 10-s intervals) and rotation rate are plotted as a function of time. During the initial 600 s segment at a fixed rotation rate of 220 rpm, the material exhibits thixotropy, with the torque decreasing by more than 50% to a nearly constant value. The rotation rate is then cycled up and down, with the torque remaining roughly constant during each "step." For some runs, the torque continues to decrease during the first few steps. However, after one- or two-step sequences, the torque at each speed becomes reproducible within approximately 0.2 Nm (replicate runs produce torque values with similar reproducibility). For the fitting results described below, only the steady data from the last decreasing–increasing–decreasing speed steps are used (illustrated in Fig. 3).

Effects of Solids Content and Reaction Temperature

The apparent shear stress–shear rate behavior is determined by averaging the torque over each rotation rate step. The first and last 10 s of each step are excluded because the rotation rate is changed gradually between steps. The average torque and rotation rate are then

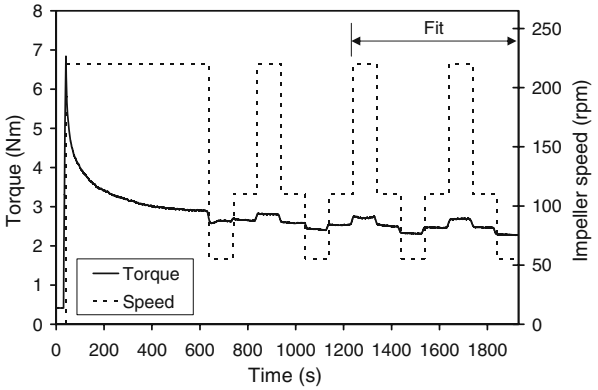

Fig. 3 Typical torque response for torque rheometer test. Hydrolysis reaction: 182 °C, 30 min, 0.5 wt.% H_2SO_4, 25 wt.% insoluble solids

converted to apparent stress and apparent shear rate using Eqs. 4 and 5, respectively. Typical results for the apparent shear stress as a function of apparent shear rate are illustrated in Fig. 4a for several biomass samples. The rheological behavior for all samples is that of a yield stress fluid, with an apparent nonzero intercept at zero shear rate. The data in Fig. 4a are replotted in Fig. 4b as apparent viscosity $\eta \equiv \tau/\dot{\gamma}$ as a function of shear rate, illustrating the shear thinning behavior of these materials.

The data in Fig. 4 suggest that the rheological behavior of the biomass sample can be represented by the Bingham model (Eq. 6). We, therefore, fit the torque–rotation rate relationship predicted by the Bingham model to the torque–rotation rate data obtained from the torque rheometer as described in the previous section. This fitting procedure gives values for the yield stress τ_0 and plastic viscosity η_{pl}. Figures 5 and 6 show the effect of stover solids concentration on the yield stress and plastic viscosity, respectively, for various hydrolysis reaction temperature at 1.0 wt.% H_2SO_4. Both properties increase with the solids content. Figures 5 and 6 are consistent with the recent results reported by Viamajala et al. [14], where the viscosity of corn-stover slurries decreased with increasing acid hydrolysis temperature.

Published correlations for the solids concentration dependence of the yield stress of fiber networks are typically of the form

$$\tau_0 = aC_m^b, \tag{9}$$

where C_m is the weight fraction of solids and a and b are empirical parameters [31–33]. Values of the parameters a and b obtained from a least squares fit of the data in Fig. 5 with Eq. 9 are listed in Table 1.

The exponent b is approximately 4, independent of temperature. This value is similar to that observed for other fiber suspensions [31–33]. Bennington et al. [32] reported exponents that ranged from 2.3 for semi-bleached Kraft wood pulp to 3.6 for thermomechanical wood pulp, indicating that b depends on the type of fiber processing. Pimenova and Hanley [13] examined the rheological properties of dilute acid hydrolyzed corn stover (hydrolysis temperature unspecified; rheological measurements at 25 °C). Bingham yield stress values obtained over the solids concentration range of 5–17 wt.% fit with Eq. 9 results in the values $a = 8.1 \times 10^4$ Pa and b=4.6. The value of the exponent b is consistent with our results. Their value of a, however, is much smaller than ours. This difference may be

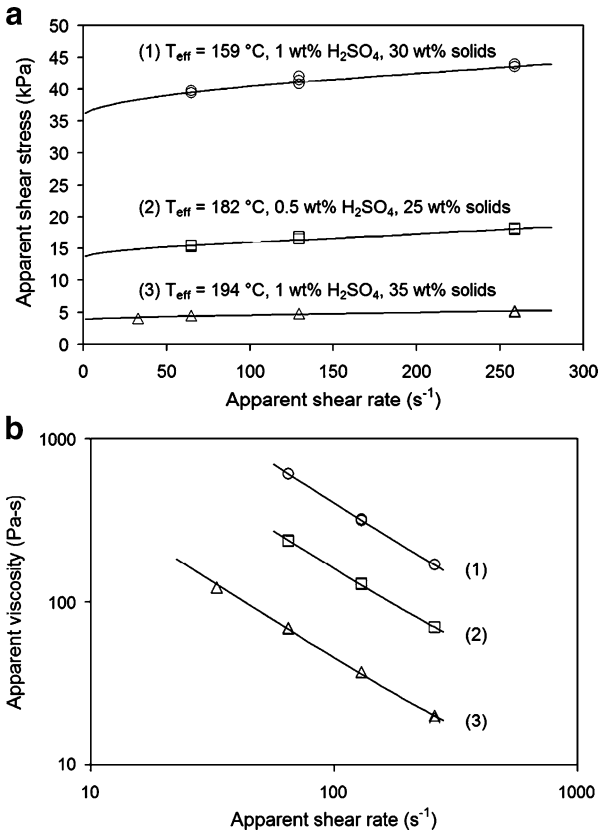

Fig. 4 **a** Apparent shear stress as a function of apparent shear rate for materials at various concentrations and processed under various conditions. The *solid curves* represent fits with the Bingham model. **b** The same data replotted as apparent viscosity as a function of apparent shear rate

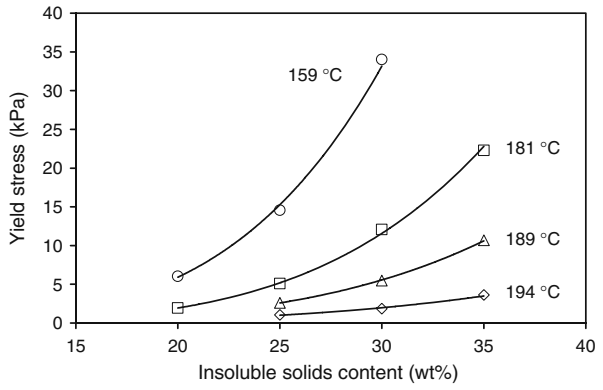

Fig. 5 Yield stress vs. solids content of acid-hydrolyzed hammer milled stover for different effective hydrolysis reaction temperatures ($T_{rheometer}$=55 °C)

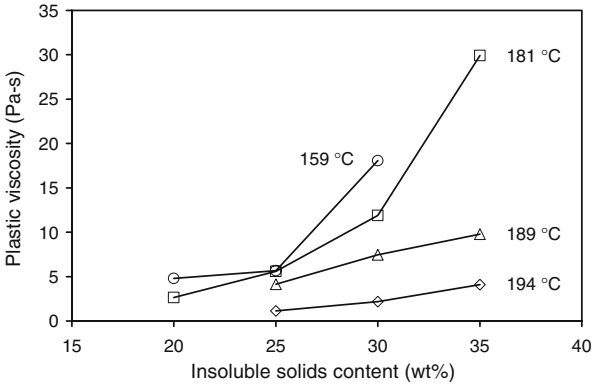

Fig. 6 Plastic viscosity vs. solids content of acid-hydrolyzed hammer milled stover for different effective hydrolysis reaction temperatures ($T_{rheometer}$=55 °C)

attributed to their fibers being significantly shorter than ours (average fiber length = 120 μm for Pimenova and Hanley's experiments, whereas we examined fibers with length greater than 300 μm and up to several centimeters; see below). The yield stress of wood fiber suspensions is commonly observed to decrease with decreasing fiber length [32, 34]. Smaller values of *a* extracted from Pimenova and Hanley's data may also be attributed in part to that fact that they apparently report concentrations as total solids (soluble plus insoluble) [14] whereas for our washed materials, the solids concentration refers to insoluble solids. We note that our yield stresses are also significantly larger than those reported by Viamajala et al. [14], who obtained maximum values of approximately 1.5 kPa, even for unhydrolyzed stover at 40 wt.% solids. This difference may also be attributed in part to smaller particle sizes employed in their study. In fact, they found that the yield stress decreased with decreasing particle size.

Table 1 illustrates that the coefficient *a* decreases with increasing reaction temperature. This suggests that fibers may decrease in size as the hydrolysis reaction temperature is increased. Washed and neutralized materials from each hydrolysis reaction were analyzed with the Pulmac Masterscreen with a 100-μm slotted screen to examine the effect of reaction temperature on particle size. When a sample is passed over the screen, particles that are sufficiently small go through the screen (termed the "accepts") and the remaining fraction of larger particles is retained on the screen (termed the "rejects"). We quantify the particle size distribution by the relative amount retained on the screen, as well as by the weight average fiber length of the accepts. The weight fraction of rejects from the screen is plotted as a function of effective reaction temperature in Fig. 7. The effect of reaction temperature on the weight average fiber length of the screen accepts, measured with a Kajaani FS100 fiber length analyzer, is illustrated in Fig. 8. Both the weight fraction of screen rejects and the average fiber length of the screen accepts decrease with increasing

Table 1 Values of the parameters *a* and *b* for acid-hydrolyzed hammer milled stover at 1.0 wt.% H_2SO_4 at $T_{rheometer}$=55 °C.

Effective Temperature (°C)	*a* (10^6 Pa)	*b*
159	5.5±0.6	4.25±0.40
181	2.3±0.1	4.40±0.17
189	0.87±0.02	4.19±0.15
194	0.17±0.02	3.69±0.70

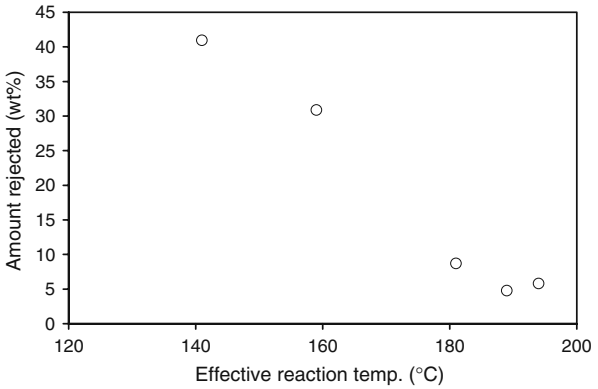

Fig. 7 Mass fraction of Pulmac screen rejects vs. effective hydrolysis temperature (30 min reaction)

reaction temperature. Thus, the decrease in yield stress with increasing reaction temperature may be caused by a decrease in particle size. However, we note that particle-level models [35–37] show that rheological properties can also be decreased by decreasing fiber stiffness; thus, other factors may contribute to the decrease in yield stress with increasing reaction temperature.

Effect of Acid Concentration

A dilute-acid hydrolysis reaction was performed at 0.5 wt.% H_2SO_4 to determine the effect of acid concentration on the apparent rheological properties of pretreated corn stover. The effective temperature of the 0.5 wt.% H_2SO_4 reaction was 182 °C, which is close to the 1.0 wt.% H_2SO_4 reaction with an effective temperature of 181 °C. The yield stress and plastic viscosity are plotted as functions of insoluble solids content for these reactions in Figs. 9 and 10, respectively. As expected, lower acid concentration results in a higher yield stress and plastic viscosity.

The weight fraction of Pulmac screen rejects and the weight average fiber length of the screen accepts for these reactions are listed in Table 2. Increased acid concentration, like

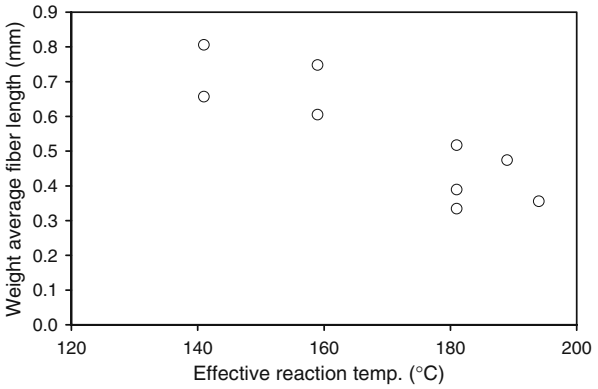

Fig. 8 Weighted average fiber length of Pulmac screen accepts vs. effective reaction temperature (30 min reaction)

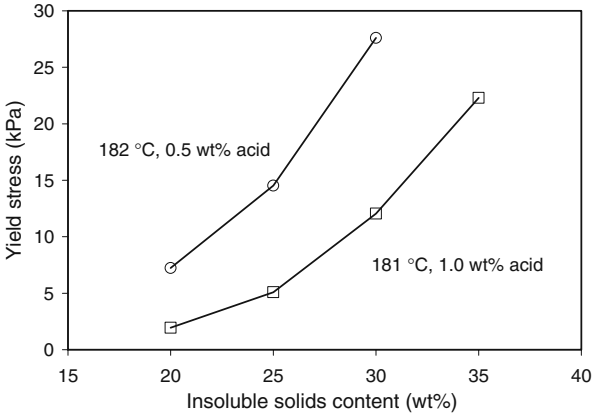

Fig. 9 Yield stress vs. solids content for two acid concentrations

increased reaction temperature, decreases the amount of material rejected by the Pulmac screen and decreases the weight average fiber length of the screen accepts.

Effect of Rheometer Temperature

The effect of rheometer temperature on rheological properties was investigated for the material hydrolyzed for 30 min at an effective reaction temperature of 181 °C with 1.0 wt.% H_2SO_4, with rheological measurements performed at 25, 30, and 35 wt.% insoluble solids. Figures 11 and 12 show the effect of rheometer temperature on the yield stress and plastic viscosity, respectively.

The yield stress decreases slightly as the rheometer temperature is increased from 25 to 65 °C. The plastic viscosity, however, is relatively insensitive to rheometer temperature. These results suggest that rheological properties of biomass need not be characterized precisely at processing temperatures.

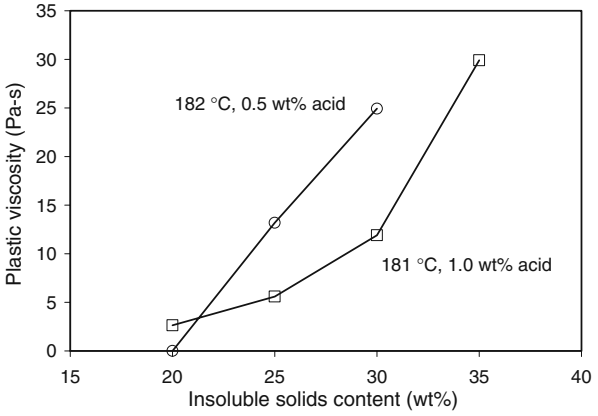

Fig. 10 Plastic viscosity vs. solids content for two acid concentrations

Table 2 Particle size as a function of H_2SO_4 concentration.

	Pulmac screen rejects (wt.%)	Weighted average fiber length (mm)
182 °C, 0.5 wt.% H_2SO_4	27	0.48
181 °C, 1.0 wt.% H_2SO_4	9	0.42

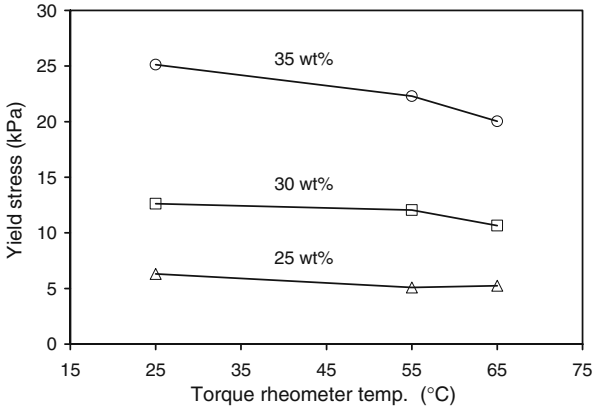

Fig. 11 Yield stress as a function of torque rheometer temperature for various solid concentrations (Hydrolysis reaction: 181 °C, 30 min, 1.0 wt.% H_2SO_4)

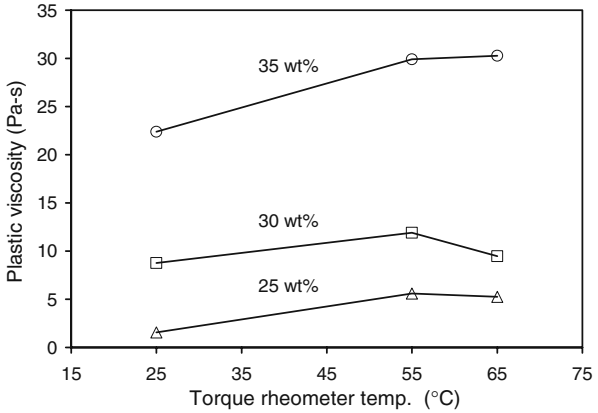

Fig. 12 Plastic viscosity as a function of torque rheometer temperature for various solid concentrations (Hydrolysis reaction: 181 °C, 30 min, 1.0 wt.% H_2SO_4)

Conclusions

The rheological properties of acid hydrolyzed corn stover slurries were investigated using torque rheometry. These materials are yield stress fluids whose rheological properties can be well represented by the Bingham model. Yield stresses increase with increasing solids concentration, and decrease with increasing hydrolysis reaction temperature, acid concentration, and rheometer temperature. At a reaction temperature of 159 °C, increasing the solids concentration from 20 to 30 wt.% causes the yield stress to increase by 460%; at a solids concentration of 30 wt.%, increasing the reaction temperature from 159 to 194 °C causes the yield stress to decrease by 95%. Plastic viscosities increase with increasing solids concentration and tend to decrease with increasing reaction temperature and acid concentration. The solids concentration dependence of the yield stress is consistent with that reported for other fibrous systems. Our results also show that effects of reaction severity on rheological properties are intimately related to changes in particle size, suggesting that studies of pretreatment methods should include measures of the influence of pretreatment on particle size.

Acknowledgments This project was supported in part by the National Research Initiative of the USDA Cooperative State Research, Education and Extension Service, grant number 2006-35504-17401.

References

1. Aden, A., Ruth, M., Ibsen, K., Jechura, J., Neeves, K., Sheehan, J., et al. (2002). NREL Technical Report TR-510-32438.
2. Schell, D. J., Farmer, J., Newman, M., & McMillan, J. D. (2003). *Applied Biochemistry and Biotechnology*, *105*, 69–85. doi:10.1385/ABAB:105:1-3:69.
3. Wooley, R., Ruth, M., Sheehan, J., Ibsen, K., Majdeski, H., & Galvez, A. (1999). NREL Technical Report TP-580-26157.
4. Sheehan, J., Aden, A., Paustian, K., Killian, K., Brenner, J., Walsh, M., et al. (2004). *Journal of Industrial Ecology*, *7*, 117–146. doi:10.1162/108819803323059433.
5. Wyman, C. E. (2007). *Trends in Biotechnology*, *25*, 153–157. doi:10.1016/j.tibtech.2007.02.009.
6. Lynd, L. R. (1996). *Annual Review of Energy and the Environment*, *21*, 403–465. doi:10.1146/annurev.energy.21.1.403.
7. Wingren, A., Galbe, M., & Zacchi, G. (2003). *Biotechnology Progress*, *19*, 1109–1117. doi:10.1021/bp0340180.
8. Jørgensen, H., Vibe-Pedersen, J., Larsen, J., & Felby, C. (2007). *Biotechnology and Bioengineering*, *96*, 862–870. doi:10.1002/bit.21115.
9. Rosgaard, L., Andric, P., Dam-Johansen, K., Pedersen, S., & Meyer, A. S. (2007). *Applied Biochemistry and Biotechnology*, *143*, 27–40. doi:10.1007/s12010-007-0028-1.
10. Um, B., & Hanley, T. R. (2008). *Applied Biochemistry and Biotechnology*, *145*, 29–38. doi:10.1007/s12010-007-8105-z.
11. Lu, Y., Wang, Y., Xu, G., Chu, J., Zhuang, Y., & Zhang, S. (2008). *Applied Biochemistry and Biotechnology* . doi:10.1007/s12010-008-8306-0.
12. Pimenova, N., & Hanley, T. (2003). *Applied Biochemistry and Biotechnology*, *106*, 383–392. doi:10.1385/ABAB:106:1-3:383.
13. Pimenova, N., & Hanley, T. (2004). *Applied Biochemistry and Biotechnology, 114*, 347–360. doi:10.1385/ABAB:114:1-3:347.
14. Viamajala, S., McMillan, J. D., Schell, D. J., & Elander, R. T. (2009). *Bioresource Technology, 100*, 925–934. doi:10.1016/j.biortech.2008.06.070.
15. Nguyen, Q. D., Akroyd, T., De Kee, D. C., & Zhu, L. (2006). *Korea–Australia Rheology Journal, 18*, 15–24.
16. Scott, C. T., & Zauscher, S. (1997). *Tappi Environmental Conference Proceedings*, pp. 739–743. Atlanta: Tappi Press.

17. Zauscher, S., Scott, C. T., Willett, J. L., & Klingenberg, D. J. (2000). *Tappi Journal, 83*, 1–10.
18. Zauscher, S. (2000). PhD Thesis, University of Wisconsin, Madison, WI, USA.
19. Ehrhardt, M. E. (2008). M.S. Thesis, University of Wisconsin, Madison, WI.
20. Hsu, D. (1995). NREL Laboratory Analytical Procedure LAP-007.
21. Vroom, K. (1957). *Pulp & Paper Magazine of Canada, 58*, 238–231.
22. Biermann, C. (1996). *Handbook of pulping and papermaking* (2nd ed.). San Diego: Academic.
23. Maloney, M., Chapman, T., & Baker, A. (1985). *Biotechnology and Bioengineering, 27*, 355–361. doi:10.1002/bit.260270321.
24. Chum, H., Johnson, D., Black, S., & Overend, R. (1990). *Applied Biochemistry and Biotechnology, 24/25*, 1–14. doi:10.1007/BF02920229.
25. Saracoglu, N., Mutlu, S., Dilmac, G., & Cavusoglu, H. (1998). *Bioresource Technology, 65*, 29–33. doi:10.1016/S0960-8524(98)00032-7.
26. Kim, S., Yum, D., & Park, S. (2000). *Bioresource Technology, 72*, 289–294. doi:10.1016/S0960-8524(99)00081-4.
27. Aguilar, R., Ramirez, J., Garrote, G., & Vazquez, M. (2002). *Journal of Food Engineering, 55*, 309–318. doi:10.1016/S0260-8774(02)00106-1.
28. Goodrich, J. E., & Porter, R. S. (1967). *Polymer Engineering and Science, 7*, 45–51. doi:10.1002/pen.760070112.
29. Bousmina, M., Ait-Kadi, A., & Faisant, J. B. (1999). *Journal of Rheology (New York, N.Y.), 43*, 415–433. doi:10.1122/1.551044.
30. Bohlin VOR Rheometer Users Manual, Malvern Instruments, Westborough, MA.
31. Swerin, A., Powell, R., & Odberg, L. (1992). *Nordic Pulp & Paper Research Journal, 7*, 126–143. doi:10.3183/NPPRJ-1992-07-03-p126-132.
32. Bennington, C., Kerekes, R., & Grace, J. (1990). *Canadian Journal of Chemical Engineering, 68*, 748–757.
33. Kerekes, R. (2006). *Nordic Pulp & Paper Research Journal, 21*, 598–612. doi:10.3183/NPPRJ-2006-21-05-p598-612.
34. Dalpke, B., & Kerekes, R. (2005). *Journal of Pulp and Paper Science, 31*, 39–43.
35. Schmid, C., Switzer, L., & Klingenberg, D. J. (2000). *Journal of Rheology (New York, N.Y.), 44*, 781–809. doi:10.1122/1.551116.
36. Switzer, L. H., & Klingenberg, D. J. (2003). *Journal of Rheology (New York, N.Y.), 47*, 759–778. doi:10.1122/1.1566034.
37. Wahren, D. (1964). *Svenska Papperstidn, 67*, 378–381.